Supporting Information

Distinct dual enzyme-like activities of Fe-N-C single-atom nanozymes enable discriminative detection of cellular glutathione

Chunqi Cai,[1†] Chengyang Zhu,[2†] Lingling Lv,[3] Pengcheng Huang,[1*] Junjie Mao,[2*] Fang-Ying Wu,[1] and Ke-Yu Deng[3]

[1]School of Chemistry and Chemical Engineering, Nanchang University, Nanchang 330031, China

[2]Key Laboratory of Functional Molecular Solids, Ministry of Education, College of Chemistry and Materials Science, Anhui Normal University, Wuhu 241002, China

[3]Institute of Translational Medicine, Nanchang University, Nanchang 330031, China

[†]These authors contributed equally to this work. *Corresponding Authors: pchuang@ncu.edu.cn (P. Huang), maochem@ahnu.edu.cn (J Mao).

Table of Contents

1. Experiment section

2. Additional figures and tables

3. References

1. Experiment section

Chemicals and Materials. All chemicals were analytical grade without any purification. Zinc nitrate hexahydrate ($Zn(NO_3)_2 \cdot 6H_2O$), iron acetylacetone and 2-methylimidazole (2-MI) were obtained from Alfa Aesar Chemical Co. Ltd. (Tianjin, China). 3,3',5,5'-tetramethylbenzidine (TMB), glutathione (GSH), sodium sulfide ninhydrate ($Na_2S \cdot 9H_2O$), ascorbic acid (AA), ₗ-homocysteine (Hcy), ₗ-cysteine (Cys), ₍DL₎-isoleucine (Ile), ₍DL₎-norvaline (Val), nitrotetrazolium blue chloride (NBT), N-ethylmaleimide (NEM), α-lipoic acid (LPA), p-phthalic acid (PTA), mannitol were purchased from Aladdin Co. Ltd. (Shanghai, China). Sodium phosphate dibasic dihydrate ($NaH_2PO_4 \cdot 2H_2O$), ₗ-tyrosine (Tyr), ₗ-proline (Pro), ₗ-phenylalanine (Phe), ₗ-arginine (Arg), ₗ-serine (Ser), ₗ-glutamic (Glu), ₗ-methionine (Met), ₗ-lysine (Lys), ₗ-histidine (His), ₗ-threonine (Thr), ₗ-alanine (Ala), ₗ-tryptophan (Try) and ₗ-aspartic (Asp) were obtained from Sinopharm Chemical Reagent Co. Ltd. (Shanghai, China). Glycine (Gly) and ₗ-leucine (Leu) were bought from Sangon Biotech Co. Ltd. (Shanghai, China). 30% Hydrogen peroxide (H_2O_2), sodium acetate trihydrate ($NaAc \cdot 3H_2O$), methanol and ethanol were obtained from Xilong Science Co. Ltd. (Guangzhou, China). 9, 10-anthracene dicarboxylic acid (H_2ADC) was purchased from Extension Co. Ltd. (Jilin, China). Dimethyl sulfoxide (DMSO) and glacial acetic acid (HAc) were purchased from Damao Chemical Reagent Factory (Tianjin, China). Disodium hydrogen phosphate dodecahydrate ($Na_2HPO_4 \cdot 12H_2O$) was obtained from Macklin Co. Ltd. (Shanghai, China). Superoxide dismutase (SOD) and the GSH assay kit were purchased from Beyotime Biotechnology Co. Ltd. (Shanghai, China). All

aqueous solutions were prepared with ultrapure water (18.2 MΩ·cm^{-1}).

Apparatus and Characterizations. UV-vis absorption spectra were measured on Cytation^{TM}3 multifunctional microplate reader (BioTek Instruments Inc., USA). Fluorescence spectra were carried out on F-4600 fluorescence spectrophotometer (Hitachi, Japan) with a 5.0 nm slit width for both excitation set and emission set. Powder X-ray diffraction (PXRD) was conducted on an X-ray diffractometer (Panalytical) utilizing Cu Kα radiation. Spin trapping electron paramagnetic resonance (EPR) were conducted by a Germany Bruker EMXplus-6/1 spectrometer at the X-band frequency (9.8 GHz) in which the Fe-N-C SAzymes (1 mg/mL) was incubated for 5 min with diluted trapping agents DMPO (100 mM) or TEMP (100 mM) in HAc-NaAc buffer (0.2 M, pH 3.5) or in methanol. Fourier transform infrared spectra (FT-IR) were done with KBr pellets on Nicolet 5700 FT-IR spectrometer (Nicolet, USA). X-ray photoelectron spectroscopy (XPS) were performed on ESCALAB250Xi photoelectron spectrometer (Thermo Fisher Scientific, USA). TEM images were recorded by JEM-2010F Transmission electron microscopy (JEOL, Japan). High-angle annular dark-field scanning TEM (HAADF-STEM) images and corresponding elemental maps were shot by aberration-corrected scanning transmission electron microscope (FEI Titan Cubed Themis G2300, Holland). X-ray absorption fine structure (XAFS) spectra were collected at 1W1B station in Beijing Synchrotron Radiation Facility (BSRF). The storage rings of BSRF were operated at 2.5 GeV with a maximum current of 250 mA. The data was collected with a Si(111) double-crystal monochromator in transmission mode using ionization chamber for Fe foil, FePc, Fe_2O_3, and in fluorescence excitation

mode using Lytle detector for Fe-N-C SAzymes. All spectra were acquired in ambient

conditions.

XAFS Analysis. The collected EXAFS data were processed according to the standard procedures using the ATHENA module implemented in the IFEFFIT software packages. The k^3-weighted EXAFS spectra were acquired by subtracting the post-edge background from the overall absorption and then normalizing with respect to the edge-jump step. Subsequently, k^3-weighted $\chi(k)$ data of Fe K-edge were Fourier transformed to real (R) space using a hanging window (dk = 1.0 Å^{-1}) to separate the EXAFS contributions from different coordination shells. To obtain the quantitative structural parameters around central atoms, least-squares curve parameter fitting was carried out using the ARTEMIS module of IFEFFIT software packages.

The following EXAFS equation was used:

$$\chi(k) = \sum_j \frac{N_j S_0^2 F_j(k)}{kR_j^2} \exp[-2k^2\sigma_j^2]\exp[\frac{-2R_j}{\lambda(k)}]\sin[2kR_j + \phi_j(k)]$$

S_0^2 is the amplitude reduction factor, $F_j(k)$ is the effective curved-wave backscattering amplitude, N_j is the number of neighbors in the jth atomic shell, R_j is the distance between the X-ray absorbing central atom and the atoms in the jth atomic shell (back scatterer), λ is the mean free path in Å, $\phi_j(k)$ is the phase shift (including the phase shift for each shell and the total central atom phase shift), σ_j is the Debye-Waller parameter of the jth atomic shell (variation of distances around the average R_j). The functions $F_j(k)$, λ and $\phi_j(k)$ were calculated with the ab initio code FEFF8.2.

Synthesis of Fe-N-C SAzymes and N-Doped Carbon Nanoparticles (N-C NPs).

Fe/ZIF-8 was synthesized through in-situ encapsulation of Fe(acac)$_3$ in the cage of ZIF-8. Briefly, Zn(NO$_3$)$_2$·6H$_2$O (1069 mg, 3.6 mmol) and Fe(acac)$_3$ (90 mg, 0.25 mmol)

were mixed in methanol (20 mL) to form a uniform solution A. 2-methylimidazole (1161 mg, 14.1 mmol) was dissolved in methanol (10 mL) to obtain a uniform solution B. Then solution A was poured into solution B with vigorous agitation for 20 min. After standing still for 20 h, the obtained product was washed with methanol for four times and dried under vacuum at 60 °C overnight to afford Fe/ZIF-8. Subsequently, Fe/ZIF-8 was transferred into a ceramic boat, placed in a tube furnace, and heated to 920 °C with a heating rate of 5 °C min^{-1} and kept at 920 °C for 3 h under Ar atmosphere. After the carbonization process, the black power of Fe-N-C SAzymes was finally obtained. The synthesis of N-C NPs was conducted with similar procedures without Fe(acac)$_3$.

Evaluation of Enzyme-Mimicking Activities of Fe-N-C SAzymes and N-C Nanoparticles. The peroxidase-like activity of Fe-N-C SAzymes and N-C NPs were investigated based on the catalytic oxidation of typical chromogenic substrate 3,3',5,5'-tetramethylbenzidine (TMB) in the presence of H_2O_2. In detail, Fe-N-C SAzymes or N-C NPs (3 μL, 0.5 mg/mL), TMB (10 μL, 5 mM), and H_2O_2 (10 μL, 100 mM) were added into 1.5 mL Eppendorf tube in sequence, and then HAc-NaAc buffer (0.2 M, pH 3.5) was added to obtain 0.5 mL of the mixed solution. After incubating for 20 min at 20 °C, the absorbance of oxidized TMB (oxTMB) at 652 nm was recorded. The oxidase-like activity of Fe-N-C SAzymes and N-C NPs were evaluated by the same procedures except for the addition of H_2O_2.

Kinetic Analysis of Fe-N-C SAzymes. The steady-state kinetic analysis of the Fe-N-C SAzymes was carried out in HAc-NaAc buffer (0.2 M, pH 3.5) containing Fe-N-C SAzymes (3 μg/mL) and various concentrations of TMB or H_2O_2. After blending

thoroughly, the absorbance at 652 nm of the mixed solution was recorded every minute. The Michaelis-Menten constant (K_m), which is an indicator reflected the affinity of the enzyme to substrate, and the maximal reaction velocity (v_{max}) were calculated according to the Lineweaver-Burk plot:

$$\frac{1}{v} = \left(\frac{K_m}{v_{max}}\right)\left(\frac{1}{[S]}\right) + \left(\frac{1}{v_{max}}\right)$$

where v is the initial velocity, K_m refers to the Michaelis constant, [S] is the concentration of the substrate, and v_{max} corresponds to the maximal reaction velocity.

Colorimetric Detection of GSH Based on the Oxidase-Like Activity of Fe-N-C SAzymes. Typically, Fe-N-C SAzymes (3 µL, 0.5 mg/mL), 5 µL of GSH at different concentrations (0.02 - 18 µM), TMB (10 µL, 5 mM), and HAc-NaAc buffer (0.2 M, pH 3.5) were added into the 1.5 mL Eppendorf tube in turn. The final volume of the mixture was fixed at 0.5 mL with the buffer. After being incubated at 20 °C for 90 min, the absorbance at 652 nm of the mixture was collected by a microplate reader.

Colorimetric Detection of GSH in Cell Lysate Samples. Beta-TC-6 cells were cultured in high-glucose DMEM supplemented with 10% fetal bovine serum and 1% double antibiotics (streptomycin and penicillin). H9C2 cells were incubated in DMEM complete medium without any supplements. The cells were cultured at 37 °C under an atmosphere containing 5% CO_2. To change the intracellular GSH level of tumor cells, Beta-TC-6 cells were pretreated with N-ethylmaleimide (NEM) (500 µM) for 1 h or α-lipoic acid (LPA) (500 µM) for 26 h.

To prepare the cell lysates, cells were digested with 0.25% trypsin and neutralized

with 3-fold amount of DMEM complete medium. Then the cells were washed with phosphate-buffered saline (PBS) and centrifuged for 3 min at 1000 rpm to acquire cell pellets. After that, the cell sedimentation was mixed with 3-fold amount of protein-removing reagent to remove the proteins in cells, followed by repeated freezing (-80 °C refrigerator) and thawing (37 °C water bath) twice. The solution was placed in ice bath for 5 min and the cell lysates were obtained by centrifuging for 10 min at 10000 rpm.

The supernatant was transferred to another tube for the following assay: Fe-N-C SAzymes (3 µL, 0.5 mg/mL), 5 µL of diluted cell lysates, TMB (10 µL, 5 mM) and HAc-NaAc buffer (0.2 M, pH 3.5) were injected into a 1.5 mL Eppendorf tube in order. The volume of the mixed solution was finalized to 0.5 mL with the buffer and then incubated at 20 °C for 90 min. The absorbance of oxTMB at 652 nm was read by a microplate reader.

2. Additional figures and tables
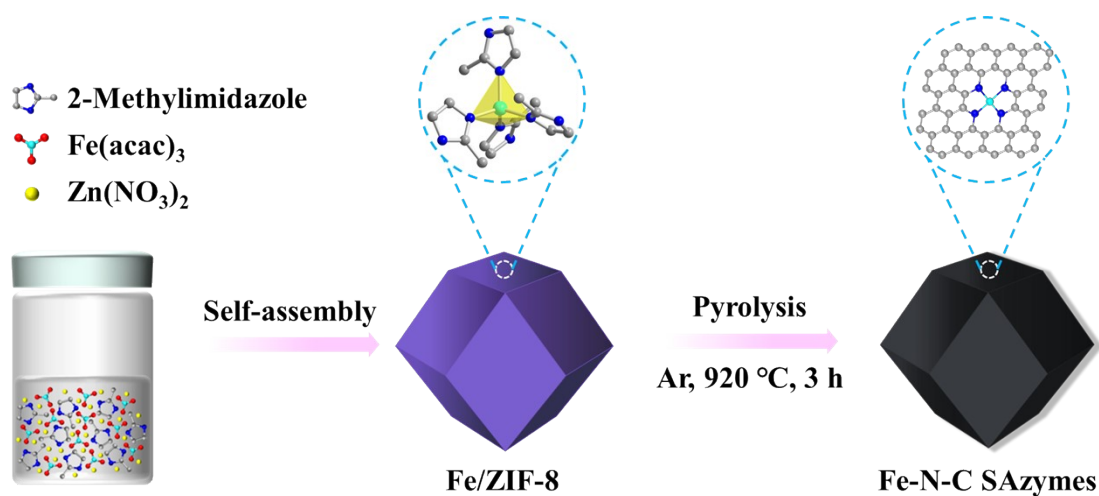
Figure S1. Schematic illustration of the synthesis route of Fe-N-C SAzymes.
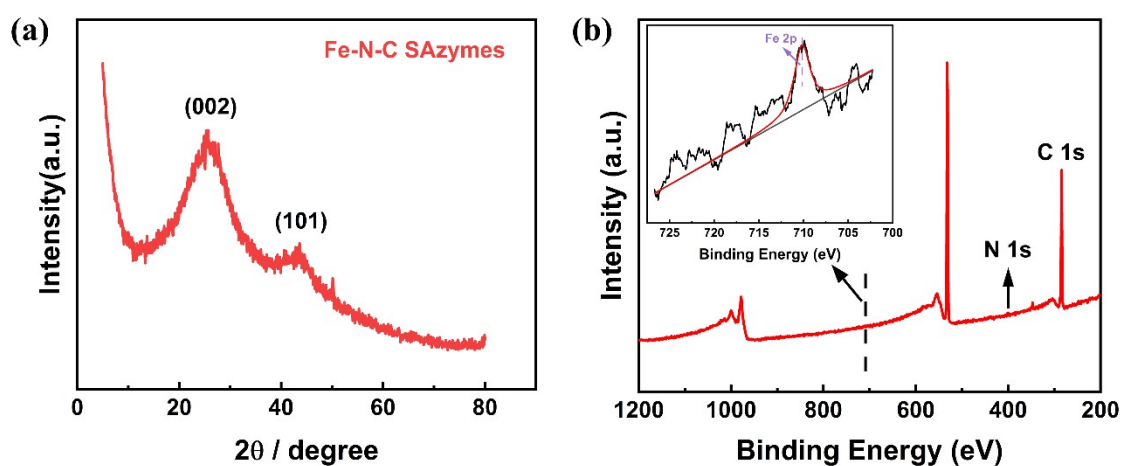
Figure S2. (a) XRD pattern of Fe-N-C. (b) XPS of Fe-N-C.

As shown in Figure S2a, the XRD pattern of Fe-N-C showed two broad peaks at around 26° and 43°, corresponding to the (002) and (101) planes of graphitic carbon,[1] indicating no XRD-detectable nanoparticles in Fe-N-C. The XPS spectrum (Figure S2b) revealed that except from the signals of C 1s and N 1s, Fe 2p signal was also detected (about 710.3 eV) with much weaker intensity, which was caused by the low atomic density of Fe.
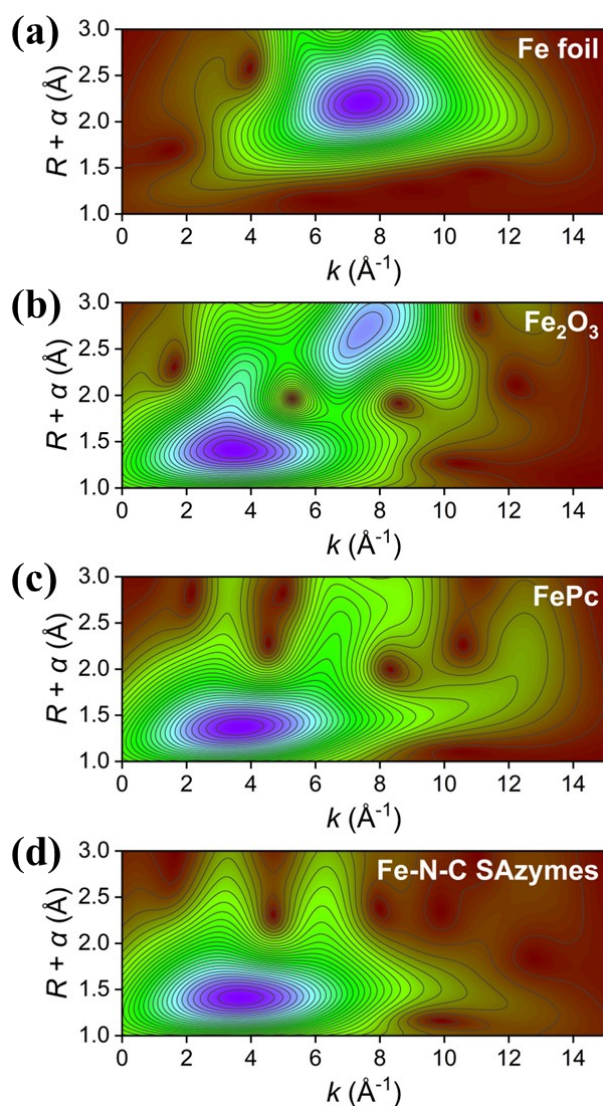
Figure S3. WT contour plots of the Fe K-edge EXAFS spectra of (a) Fe foil, (b) Fe2O3, (c) FePc standards and (d) Fe-N-C SAzymes.

As shown in Figure S3, different from the WT contour plots of the references Fe_2O_3 and Fe foil with intensity maxima at 3.8 and 7.7 $Å^{-1}$ corresponding to the contributions of Fe-O and Fe-Fe, respectively, only one intensity maximum at 3.7 $Å^{-1}$ in Fe-N-C WT contour plot appeared, which could be assigned to the link of Fe-N, indicating the absence of Fe-Fe bonding in Fe-N-C but the existence of the atomically dispersed Fe atoms.
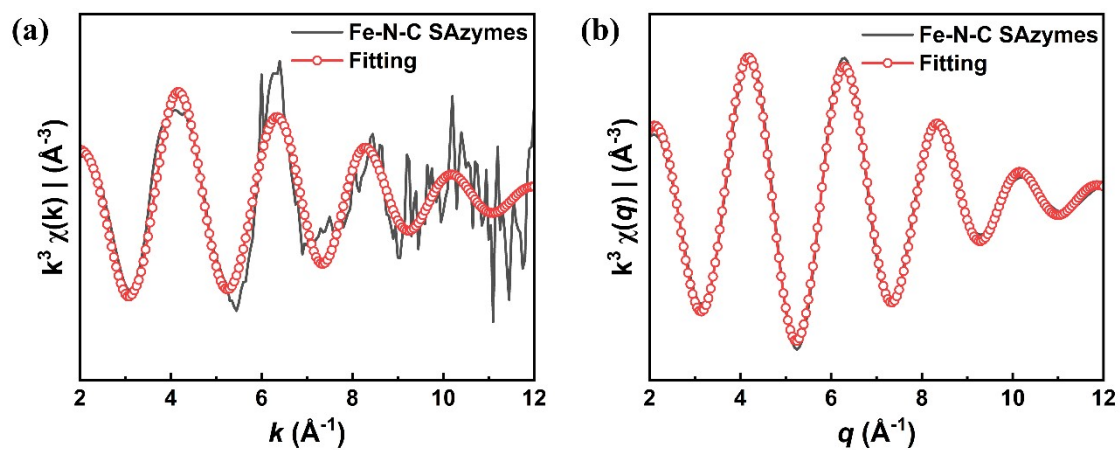
Figure S4. The corresponding XANES fitting curves of Fe-N-C SAzymes at *k* space

(a) and *q* space (b).
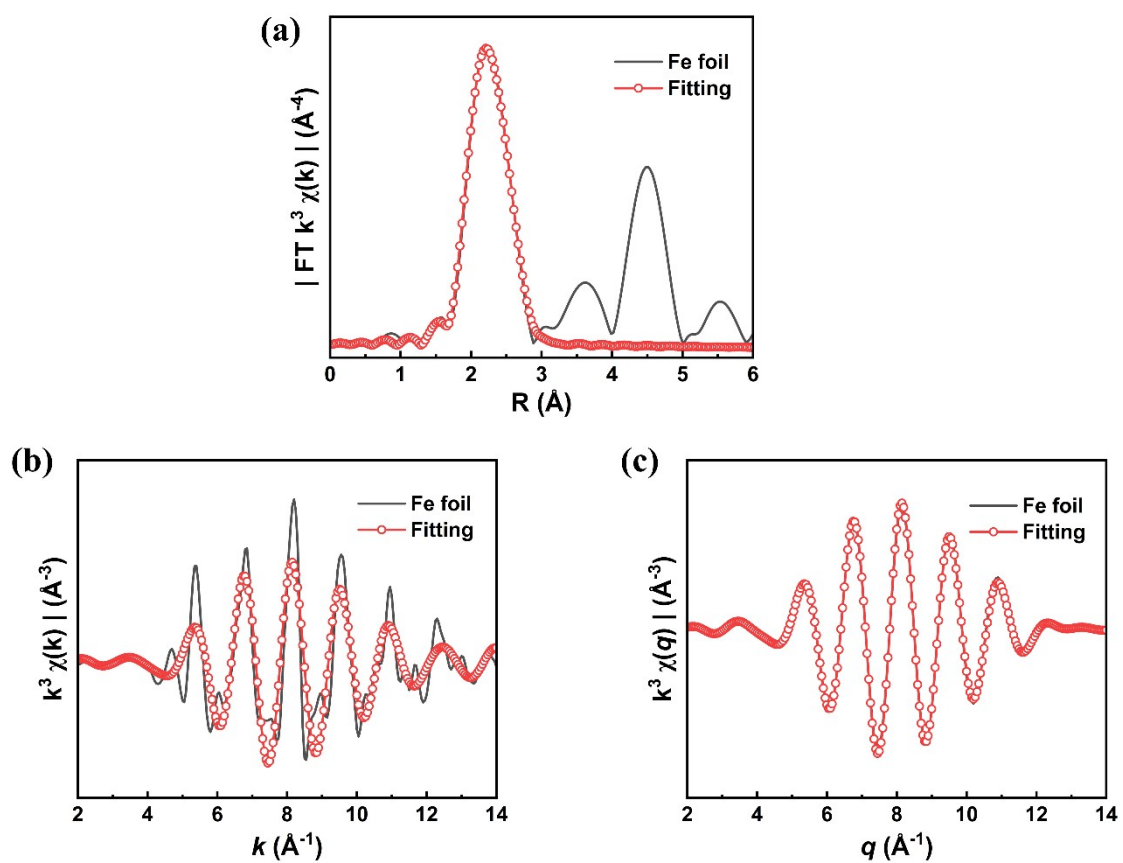
Figure S5. The corresponding Fourier-transformed EXANS fitting curves of Fe foil in

R-space (a), *k*-space (b) and *q*-space (c).

Table S1. Structural parameters extracted from the Fe K-edge EXAFS fitting. (S_0^2=0.77)

Sample	Scattering pair	CN	R(Å)	$\sigma^2(10^{-3}\text{Å}^2)$	ΔE_0(eV)	R factor
Fe-N-C SAzymes	Fe-N	3.98	2.01	10.5	0.19	0.008
Fe foil	Fe-Fe1	8*	2.46	5.6	4.45	0.006
	Fe-Fe2	6*	2.84	7.5		

S_0^2 is the amplitude reduction factor; CN is the coordination number; R is interatomic distance (the bond length between central atoms and surrounding coordination atoms); σ^2 is Debye-Waller factor (a measure of thermal and static disorder in absorber-scatterer distances); ΔE_0 is edge-energy shift (the difference between the zero kinetic energy value of the sample and that of the theoretical model). R factor is used to value the goodness of the fitting.

* This value was fixed during EXAFS fitting, based on the known structure.

Error bounds that characterize the structural parameters obtained by EXAFS spectroscopy were estimated as N ± 20%; R ± 1%; σ^2 ± 25%; ΔE_0 ± 10%.

Fe-N-C SAzymes (FT range: 2.0-10.8 Å^{-1}; fitting range: 1.1-2.1 Å)

Fe foil (FT range: 2.0-12.0 Å^{-1}; fitting range: 1-3 Å)
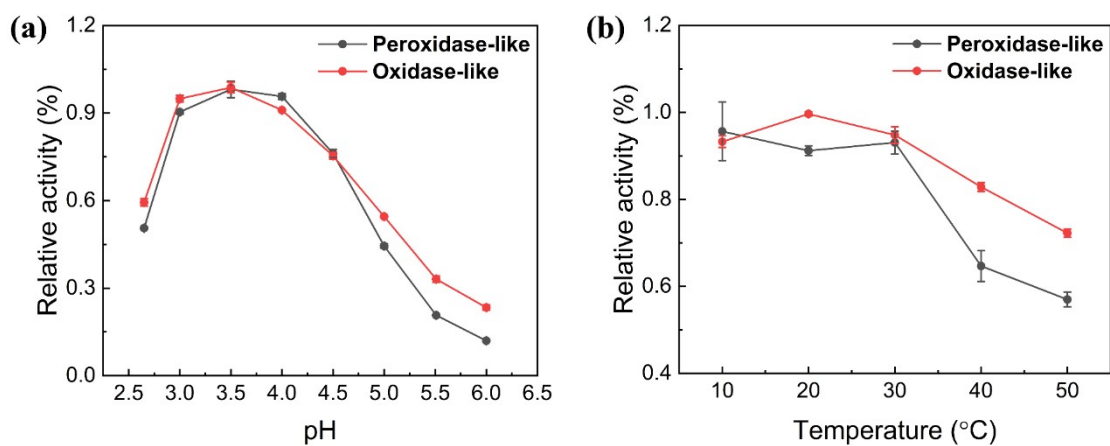
Figure S6. Effects of pH (a) and temperature (b) on the peroxidase-like and oxidase-like activities of Fe-N-C SAzyme.

As shown in Fig. S6a, both the POD-like and OXD-like activities of Fe-N-C were the highest at pH 3.5. Besides, the catalytic activities showed the maximum at 20 $^\circ$C and decreased sharply when the temperature was higher than 30 $^\circ$C (Fig. S6b). Especially, the OXD-like activity of Fe-N-C was more stable than the POD-like activity, which is mainly due to poor stability of H_2O_2 under high temperature and basic medium.
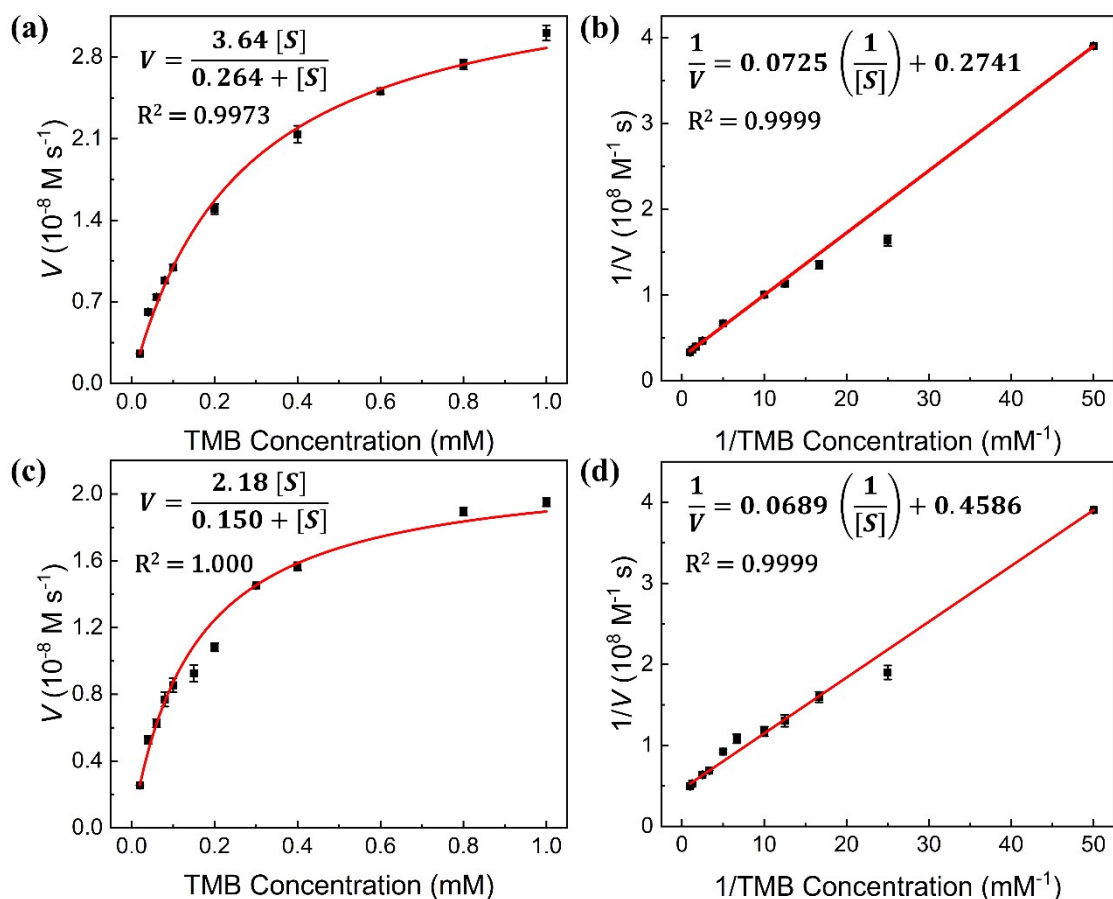
Figure S7. Steady-state kinetic assay for the peroxidase-like (a) and oxidase-like (c) activity of Fe-N-C SAzymes by varied the concentration of TMB. Double-reciprocal plot of the peroxidase-like (b) and oxidase-like (d) activity of Fe-N-C SAzymes with TMB as the substrate.

Table S2. Kinetics parameters of Fe-N-C SAzymes and HRP.

Catalyst	Substance	K_m (mM)	v_{max} (Ms^{-1})	Ref.
Fe-N-C SAzymes (Peroxidase-like）	TMB	0.264	3.64×10^{-8}	
Fe-N-C SAzymes （Oxidase-like）	TMB	0.150	2.18×10^{-8}	This work
HRP	TMB	0.434	10.0×10^{-8}	[2]
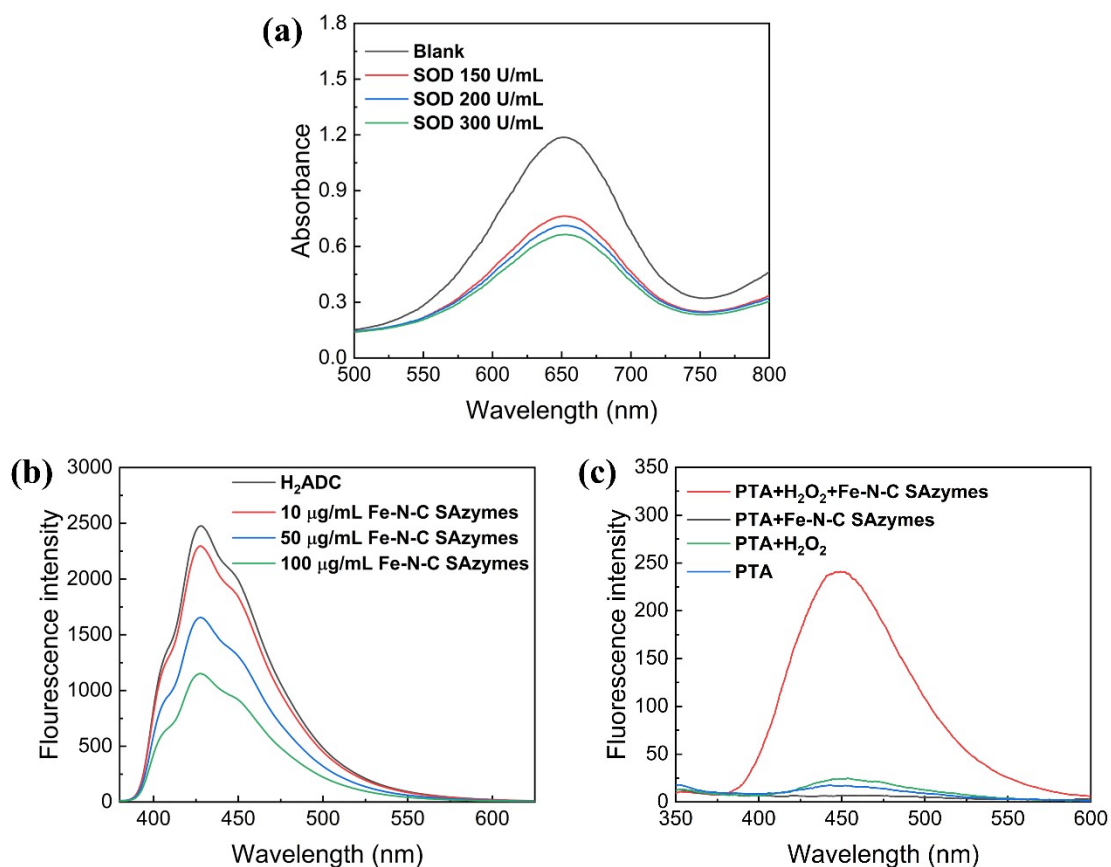
Figure S8. (a) The effect of SOD with different concentrations on Fe-N-C SAzymes - TMB reaction system. (b) Fluorescence spectra of H_2ADC in the absence and presence of Fe-N-C SAzymes with varied concentrations. (c) Fluorescence spectra of PTA + H_2O_2 + Fe-N-C SAzymes, PTA + Fe-N-C SAzymes, PTA + H_2O_2 and PTA in PBS buffer (10 mM, pH 7.4).

As shown in Fig.S8a, the more targeted scavenger superoxide dismutase (SOD) was used to further confirm the production of $O_2^{\cdot-}$ during the OXD-like catalysis. Consistent with the inhibition of NBT, SOD largely suppressed the OXD-like activity of Fe-N-C. Additionally, $^1O_2$-specific fluorescence probe 9, 10-anthracene dicarboxylic acid (H_2ADC) was selected to affirm the production of $^1O_2$. As shown in Fig. S8b, the fluorescence of H_2ADC was quenched sharply with the increase of Fe-N-C in the OXD-

like catalytic system, which verified the generation of $^1O_2$. On the other hand, only when Fe-N-C coexisted with H_2O_2, there appeared a strong emission peak of 2-hydroxy terephthalic acid (TAOH) at 450 nm, while no characteristic emission peak of TAOH was observed in the absence of H_2O_2 (Fig. S8c), implying that no ·OH existed in OXD-like catalytic system.
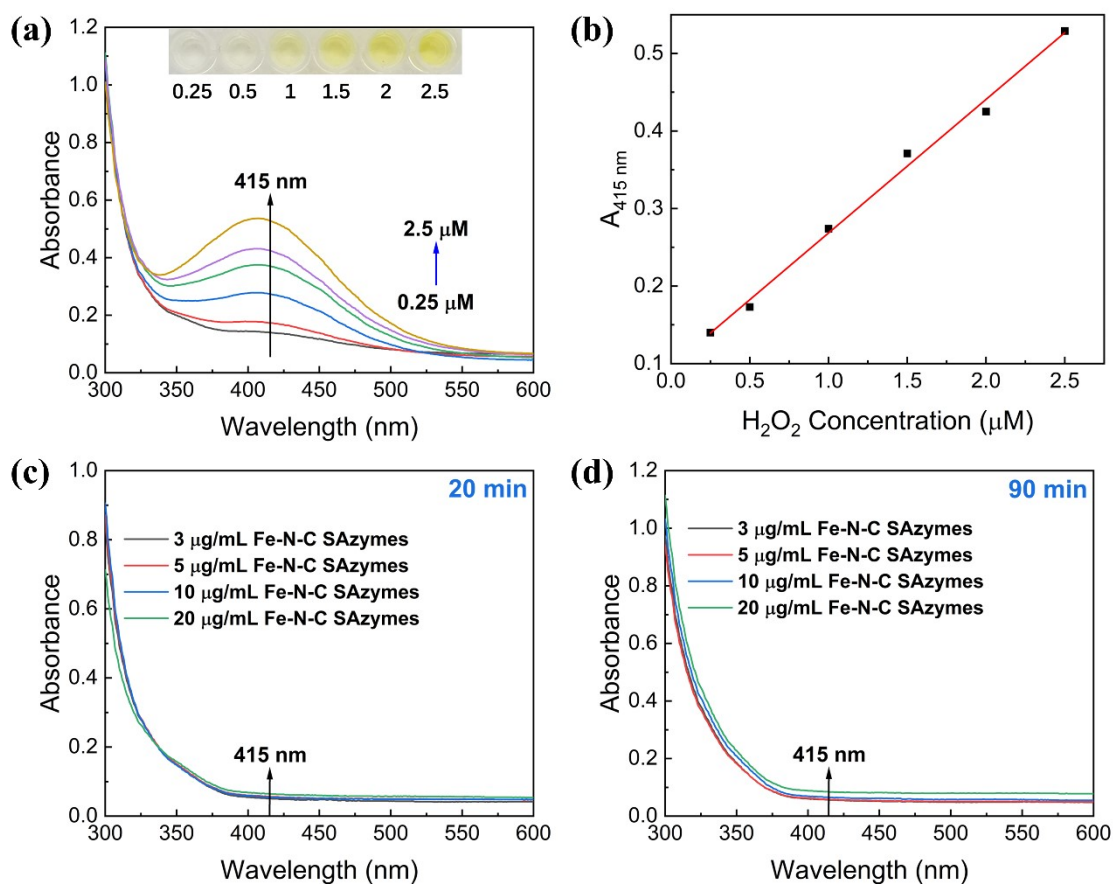
Figure S9. (a) UV-vis absorption spectra of peroxide-titanium complex formed by the reaction of titanium sulfate (Ti(SO$_4$)$_2$) with H$_2$O$_2$ at different concentrations (0.25-2.5 µM). Inset: corresponding photographs of six samples. (b) Linear calibration curve of absorbance at 415 nm versus H$_2$O$_2$ in the concentration range of 0.25 to 2.5 µM. UV-vis absorption spectra for detecting H$_2$O$_2$ with Fe-N-C SAzymes at different concentrations at the reaction time for 20 min (c) and 90 min (d).

H$_2$O$_2$ content assay kit: Under strong acidic medium, H$_2$O$_2$ could react with Ti(SO$_4$)$_2$ to produce a yellow peroxide-titanium complex precipitation with a characteristic absorption peak at 415 nm. The content of H$_2$O$_2$ can be detected quantitatively by recording the absorbance at 415 nm.
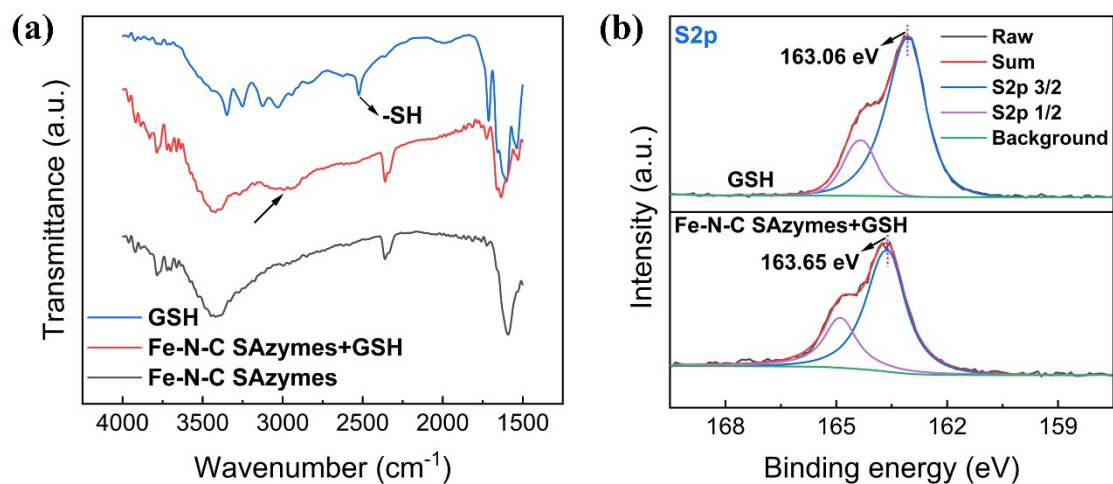
Figure S10. (a) FTIR spectra of GSH, GSH-treated Fe-N-C SAzymes and the Fe-N-C SAzymes. (b) S 2p high-resolution XPS spectra for GSH in the absence and presence of Fe-N-C SAzymes.

As shown in Figure S10a, after being treated by GSH, Fe-N-C exhibited a new small peak at ca. 3000 cm^{-1}, which could be caused by the Fe-S coordination bond.[3] Meanwhile, the characteristic absorption peak of thiols at about 2500 cm^{-1} disappeared, which also confirmed robust coordination between S atoms of GSH and Fe atoms of Fe-N-C. XPS for S atoms of GSH and GSH-treated Fe-N-C (Fig. S10b) revealed that the S 2p peak was shifted toward a higher binding energy for about 0.6 eV, further verifying high affinity between GSH and Fe atoms.
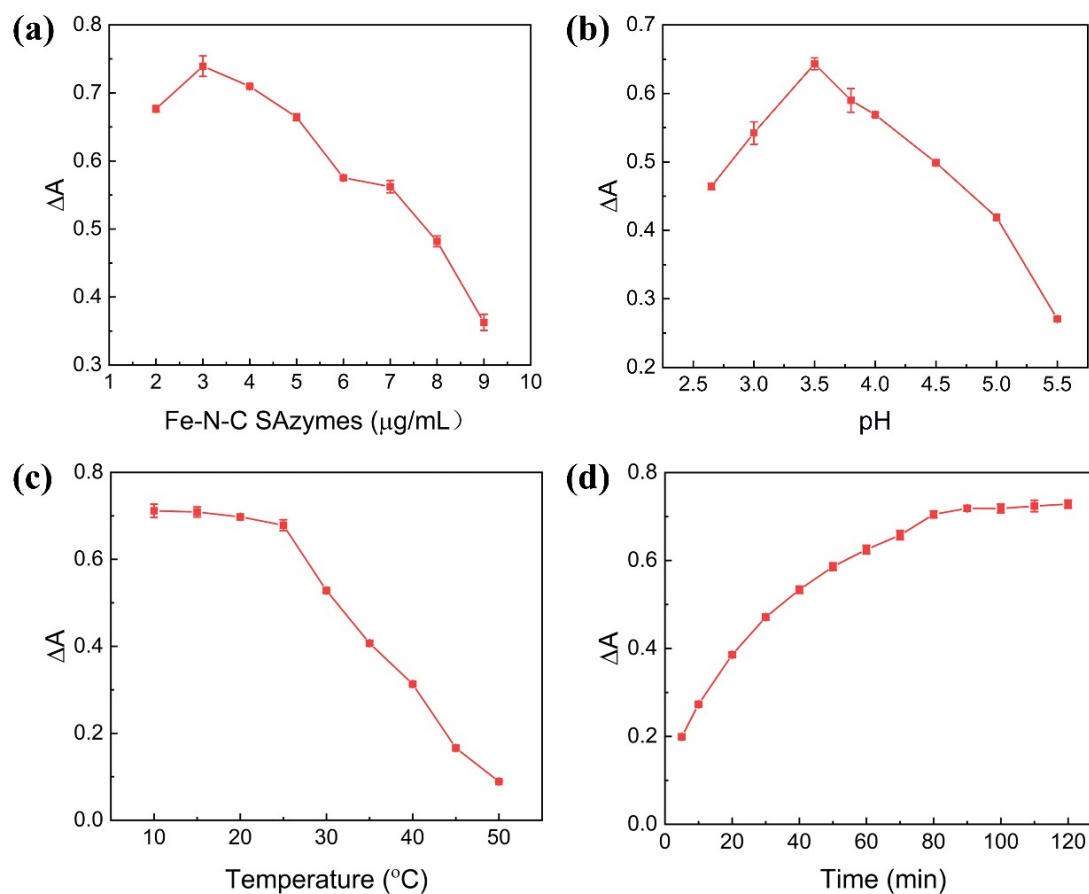
Figure S11. The dependence of the ΔA of the Fe-N-C SAzymes-TMB sensing system on the concentration of Fe-N-C SAzymes (a), pH (b), temperature (c) and incubation time (d). ΔA ($= A_0 - A$) was a parameter to optimize the sensing conditions, where A_0 and A were the absorbance at 652 nm in the absence and presence of GSH, respectively.

Several important parameters affecting the detection of GSH were investigated, including the concentration of Fe-N-C SAzymes, pH, reaction temperature and incubation time. As shown in Figure S11, 3 μg/mL Fe-N-C SAzymes, pH 3.5, 20 °C and 90 min incubation time were the optimal reaction conditions for GSH detection.
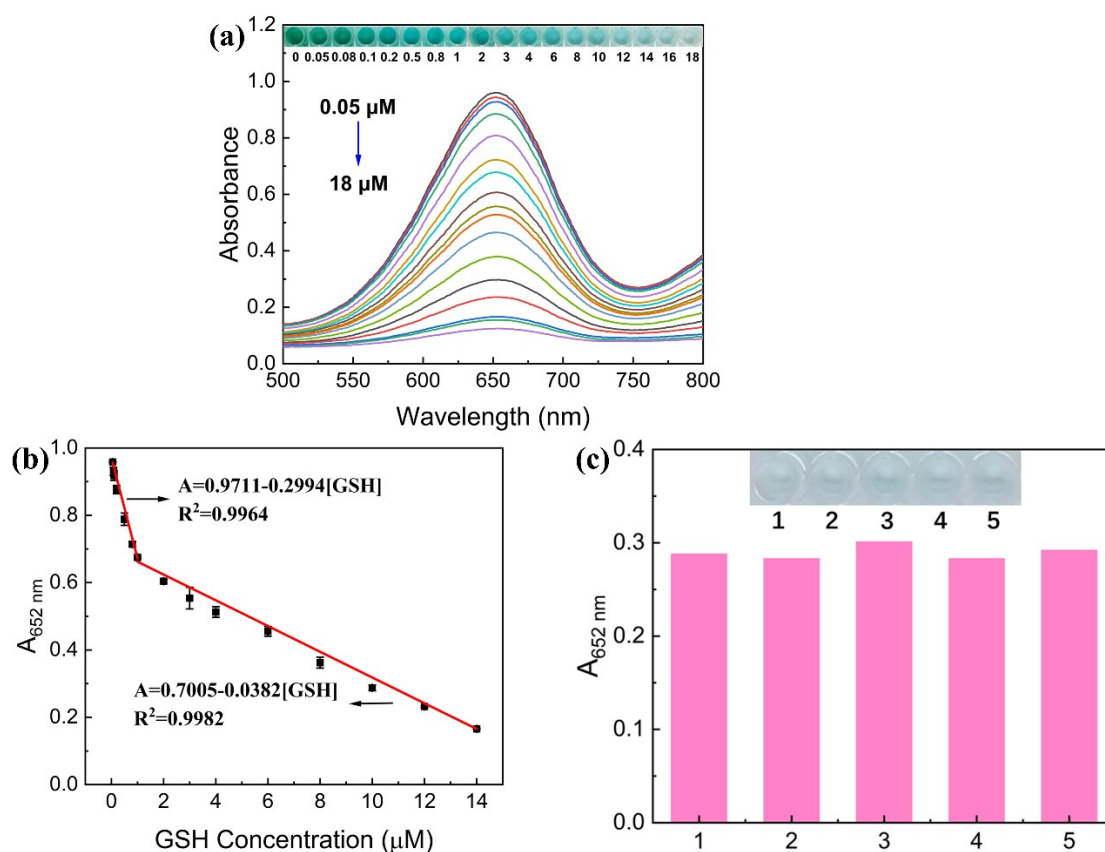
Figure S12. (a) UV-vis absorption spectra of TMB catalytically oxidized by the Fe-N-C SAzymes in the presence of GSH at different concentrations (0.05-18 μM). Inset: corresponding photograph. (b) Linear calibration plot in the concentration range from 0.05 to 14 μM. (c) The reproducibility of this assay testified by five detections of GSH (12 μM). Inset: corresponding photographs.

Table S3. Comparison of different nanozyme-based colorimetric methods for GSH detection.

Materials	Enzyme-like	Specificity to GSH	Linear range (μM)	LOD (μM)	Ref.
Ag@MnO$_2$	Oxidase	NA	0.1-55	0.08	[4]
COF-300-AR	Oxidase	Low	1-15	1.0	[5]
PSMOF	Oxidase	Low	1-20	0.68	[6]
Meso-MnO$_2$ wire	Oxidase	Low	0.3-15	0.11	[7]
Ir/NC	Oxidase	Low	0.05-15	0.5	[8]
MnO$_2$ nanosheets	Oxidase	Low	1-25	0.3	[9]
Ce-MOF (MVCM)	Oxidase	Low	0-40	0.129	[10]
UiO-66(NH$_2$) NPs	Oxidase	Low	5-120	0.31	[11]
Ag$^+$–TMB	Oxidase	High	0.05-8	0.05	[12]
MNPG	Oxidase	High	0.2-20	0.05	[13]
PtNPs@MnO$_2$	Oxidase	Low	0.2-11	0.05	[14]
NiV$_2$O$_6$	Peroxidase	Low	3-100	0.89	[15]
Au Nanoclusters	Peroxidase	Low	2-25	0.42	[16]
SWCNTs@MoS$_2$	Peroxidase	Low	0.01-1000	0.007	[17]
Pd–Fe$_3$O$_4$ DBNPs	Peroxidase	Low	0.25-1.5	0.137	[18]
IrO$_2$/rGO nanocomposites	Peroxidase	Low	0.1-50	0.083	[19]
H$_2$TCPP−TiO$_2$−MMT	Peroxidase	Low	1-20	0.057	[20]
MP-GO-hemin	Peroxidase	NA	10^{-4}-1.0	8.2×10^{-5}	[21]
Fe$_3$O$_4$ MNPs	Peroxidase	High	3-30	3.0	[22]
Fe$_3$O$_4$/MIL-88	Peroxidase	High	0-3	0.0369	[23]
Fe-N-C SANs	Peroxidase & Oxidase	NA	100-400	78.33	[24]
Fe-N-C SAzymes	Peroxidase & Oxidase	High	0.05-14	0.0396	This work
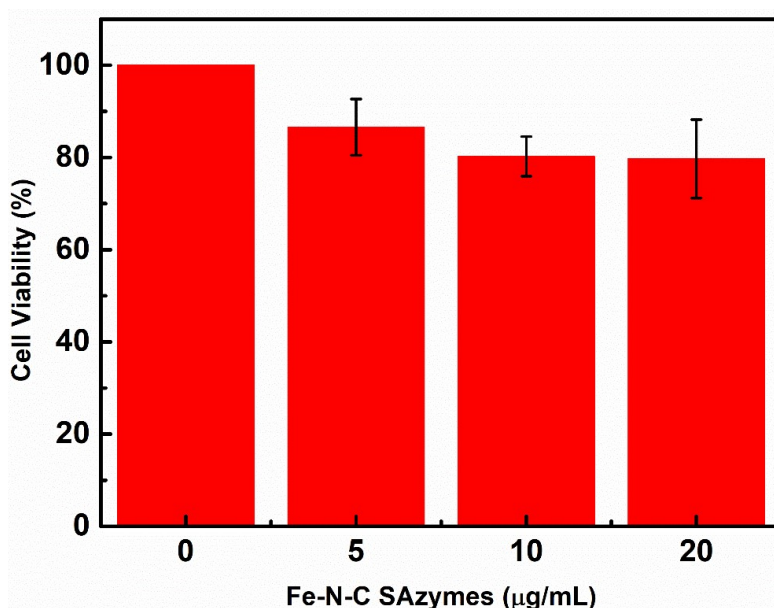
Figure S13. Cytotoxicity of Fe-N-C on Beta-TC-6 cells determined by CCK-8 assay.
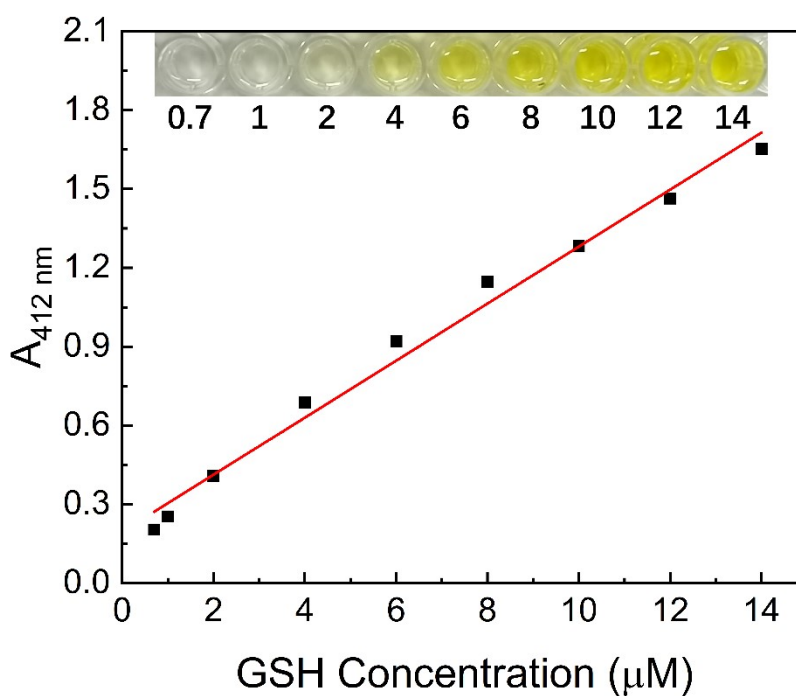
Figure S14. Calibration curve of the GSH assay kit in the concentration range from 0.7

to 14 µM. Inset: photographs of corresponding solutions.

Commercial GSH assay kit: The GSH kit is based on the exchange reactions between

sulfhydryl group of GSH and 5,5'-dithio-bis-2-nitrobenzoic acid (DTNB) and

accompanied with the generation of a yellow-colored product of 5-thio-2-nitrobenzoic acid (TNB). Measurement of the absorbance of TNB at 412 nm can be employed to quantify the GSH level of the sample.

Table S4. Cellular GSH levels evaluated by oxidase-like Fe-N-C SAzymes and commercial GSH assay kit.

Cell	Our Approach (mM)	GSH Assay Kit (mM)
Beta-TC-6	3.80 ± 0.24	3.84 ± 0.16
H9C2	0.623 ± 0.051	0.582 ± 0.11

Table S5. Results of GSH content in Beta-TC-6 cell lysate samples under different stimulations.

Samples	Our Approach (mM)	GSH Assay Kit (mM)
Control	3.46 ± 0.30	3.91 ± 0.26
+NEM	0.408 ± 0.087	0.488 ± 0.031
+LPA	4.09 ± 0.16	4.46 ± 0.19

Table S6. Comparison of our approach and GSH assay kit in five aspects.

	Color visibility	Convenience (Step)	Linear range (µM)	Sensitivity (nM)	Specificity
Our Approach	Green/Blue/Colorless	3×3	0.05-14	39.6	GSH
GSH Assay Kit	Colorless/Yellow	7×4	0.7-14	500	S^{2-}/GSH/Cys/Hcy

Convenience: number of pre-prepared solutions × number of addition of solutions to the detection system.
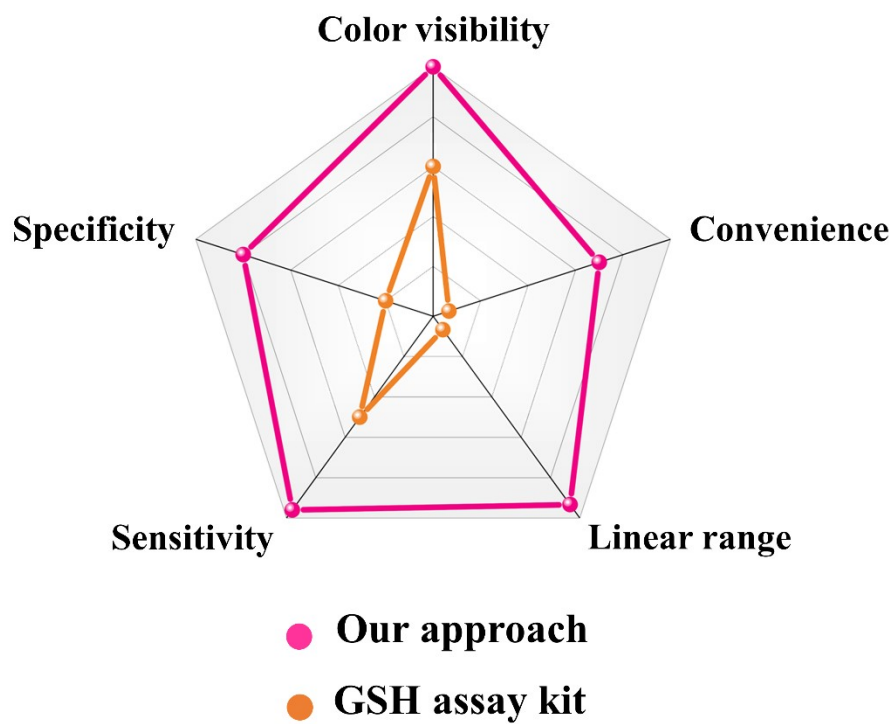
Figure S15. Comparison between our approach and GSH assay kit.

3. References

(1) Chen, Y.; Ji, S.; Wang, Y.; Dong, J.; Chen, W.; Li, Z.; Shen, R.; Zheng, L.; Zhuang, Z.; Wang, D.; Li, Y. *Angew. Chem. Int. Ed.* **2017**, *56*, 7003.

(2) Gao, L.; Zhuang, J.; Nie, L.; Zhang, J.; Zhang, Y.; Gu, N.; Wang, T.; Feng, J.; Yang, D.; Perrett, S.; Yan, X. *Nat. Nanotechnol.* **2007**, *2*, 577-583.

(3) Wu, Y.; Jiao, L.; Luo, X.; Xu, W.; Wei, X.; Wang, H.; Yan, H.; Gu, W.; Xu, B. Z.; Du, D.; Lin, Y.; Zhu, C. *Small* **2019**, *15*, 1903108.

(4) Tian, L.; Huang, Z.; Na, W.; Liu, Y.; Wang, S.; He, Y.; Cheng, W.; Huang, T.; Li, Z.; Li, T. *Nanoscale* **2022**, *14*, 15340-15347.

(5) Jin, P.; Niu, X.; Zhang, F.; Dong, K.; Dai, H.; Zhang, H.; Wang, W.; Chen, H.; Chen, X. *ACS Appl. Mater. Interfaces* **2020**, *12*, 20414-20422.

(6) Liu, Y.; Zhou, M.; Cao, W.; Wang, X.; Wang, Q.; Li, S.; Wei, H. *Anal. Chem.* **2019**, *91*, 8170-8175.

(7) Zhang, X.; Mao, X.; Li, S.; Dong, W.; Huang, Y. *Sens. Actuators B* **2018**, *258*, 80-87.

(8) Huang, M.; Wang, H.; He, D.; Jiang, P.; Zhang, Y. *Chem. Commun.* **2019**, *55*, 3634-3637.

(9) Liu, J.; Meng, L.; Fei, Z.; Dyson, P. J.; Jing, X.; Liu, X. *Biosens. Bioelectron.* **2017**, *90*, 69-74.

(10) Xiong, Y.; Chen, S.; Ye, F.; Su, L.; Zhang, C.; Shen, S.; Zhao, S. *Chem. Commun.* **2015**, *51*, 4635-4638.

(11) Hu, Z.; Jiang, X.; Xu, F.; Jia, J.; Long, Z.; Hou, X. *Talanta* **2016**, *158*, 276-282.

(12) Ni, P.; Sun, Y.; Dai, H.; Hu, J.; Jiang, S.; Wang, Y.; Li, Z. *Biosens. Bioelectron.* **2015**, *63*, 47-52.

(13) Zhang, H.; Chen, J.; Yang, Y.; Wang, L.; Li, Z.; Qiu, H. *Anal. Chem.* **2019**, *91*, 5004-5010.

(14) Liu, J.; Meng, L.; Fei, Z.; Dyson, P. J.; Zhang, L. *Biosens. Bioelectron.* **2018**, *121*, 159-165.

(15) Zhu, Q.; Yang, J.; Peng, Z.; He, Z.; Chen, W.; Tang, H.; Li, Y. *Talanta* **2021**, *234*, 122645.

(16) Feng, J.; Huang, P.; Shi, S.; Deng, K.-Y.; Wu, F.-Y. *Anal. Chim. Acta* **2017**, *967*, 64-69.

(17) Feng, L.; Zhang, L.; Chu, S.; Zhang, S.; Chen, X.; Gong, Y.; Du, Z.; Mao, G.; Wang, H. *Anal. Chim. Acta* **2022**, *1221*, 340083.

(18) Duan, W.; Qiu, Z.; Cao, S.; Guo, Q.; Huang, J.; Xing, J.; Lu, X.; Zeng, J. *Biosens. Bioelectron.* **2022**, *196*, 113724.

(19) Liu, X.; Wang, X.; Han, Q.; Qi, C.; Wang, C.; Yang, R. *Talanta* **2019**, *203*, 227-234.

(20) Zhu, X.; Li, H.; Zhang, D.; Chen, W.; Fu, M.; Nie, S.; Gao, Y.; Liu, Q. *ACS Sustain. Chem. Eng*. **2019**, *7*, 18105-18113.

(21) Bi, S.; Zhao, T.; Jia, X.; He, P. *Biosens. Bioelectron.* **2014**, *57*, 110-116.

(22) Ma, Y.; Zhang, Z.; Ren, C.; Liu, G.; Chen, X. *Analyst*, **2012**,*137*, 485-489.

(23) Zhang, Y.; Zhang, W.; Chen, K.; Yang, Q.; Hu, N.; Suo, Y.; Wang, J. *Sens. Actuators B* **2018**, *262*, 95-101.

(24) Lu, W.; Chen, S.; Zhang, H.; Qiu, J.; Liu, X. *J. Materiomics* **2022**, *8*, 1251-1259.